Original Article
Downregulation of microRNA-16-5p accelerates fracture healing by promoting proliferation and inhibiting apoptosis of osteoblasts in patients with traumatic brain injury

Yun Sun[2*], Yuan Xiong[1*], Chenchen Yan[1], Lang Chen[1], Dong Chen[1], Bobin Mi[1], Guohui Liu[1]

Departments of [1]Orthopaedics, [2]Neurosurgery, Union Hospital, Tongji Medical College, Huazhong University of Science and Technology, Wuhan 430022, China. *Equal contributors.

Abstract: Patients who suffered a traumatic brain injury (TBI) show a faster fracture healing than patients with isolated fractures. Prior studies have suggested that this process may be accelerated through the inhibition of key microRNAs. In this study, we aimed to explore the mechanisms underlying this phenomenon, with a special focus on miR-16-5p, which is markedly decreased in patients with TBI. In vitro, miR-16-5p over-expression significantly inhibited cell proliferation in MC3T3-E1 cells transfected with agomiR-16-5p. Flow cytometry analysis further demonstrated that the overexpression of miR-16-5p induced cell cycle G1/S phase arrest and apoptosis. Moreover, target prediction and luciferase reporter assay demonstrated that miR-16-5p could negatively regulate Bcl-2 and Cyclin-D1 expression. Meanwhile, Bcl-2 and Cyclin-D1 were up-regulated after osteogenic differentiation while the down-regulation of endogenous Bcl-2 and Cyclin-D suppressed the osteogenic differentiation of MC3T3-E1 cells. In vivo, PBS, agomiR-16-5p and antagomiR-16-5p were injected into fracture sites to assess any improvements in fracture healing, which further confirmed the negative effect of miR-16-5p on fracture healing. Together, these results demonstrate miR-16-5p downregulation may accelerate fracture healing by enhancing the proliferation and inhibiting the apoptosis of osteoblasts in patients with both fractures and TBI. These phenomena may be exploited in the treatment of fractures.

Keywords: Traumatic brain injury, fracture, miRNA

Introduction

Patients with fractures and concomitant traumatic brain injuries (TBI) are frequent trauma cases. Faster fracture healing in these patients has been widely recognized in comparison to those with isolated bone fractures. Numerous research in the past decades have shown that TBI is associated with rapid callus formation and bone fracture healing [1-5]. However, the mechanisms underlying this phenomenon are still unclear.

Fracture healing involves several cellular and biochemical processes, including formation of a hematoma along with inflammation, endochondral ossification, and bone remodeling [6, 7]. The latter stage is key, with osteoblasts being the primary mediators of bone formation [8, 9]. Recently, the role of microRNAs (miRNAs)-

short, noncoding single-strand RNAs-have been characterized in fracture healing, where they have been shown to inhibit osteoblast differentiation and bone formation by targeting osteogenic factors [10-12].

Indeed, suppressive miRNAs have been observed to modulate osteogenic signaling, osteoblast growth, and bone formation in humans [13-15]. Downregulation of miR-367-5p has been recognized to promote osteoblast proliferation and growth in microgravity-induced bone healing in which Pannexin-3 (PANX3), a structural component of the gap junctions and hemichannels, was shown to be the direct target of miR-367-5p [16]. On the other hand, a study [10] has indicated that miR-148a-5p could suppress osteoblast differentiation by targeting the insulin-like growth factor 1 (IGF1). Many other biomolecules have also been link-

ed with miRNA modulation and osteoblast differentiation [17-20]. Both miR-130a-3p and miR-27a-5p have been associated with osteogenesis, by appearing to potentiate the expression of Runx2, Osterix, Col1a1, as well as the alkaline phosphatase activity [21].

Bcl-2 is known to act as an anti-apoptotic molecule in multiple cell systems, including factor-dependent lymphohematopoietic and neural cells, where it can modulate mitochondrial membrane permeability and caspase activity by preventing the mitochondrial release of cytochrome c and binding to the apoptosis-activating factor (APAF-1) [29]. Overexpression of Bcl-2 has been associated with decreased osteoblast apoptosis and elevated osteoblast marker genes [23]. Molecular structural studies have also corroborated that Bcl-2 is associated with the osteoblast apoptosis [22, 24].

Cyclin-D1 can regulate cyclin D1-CDK4 (DC) complex activity, modulating phosphorylation and the inhibition of several molecules in the retinoblastoma (RB) protein, thereby regulating the G(1)/S transition within the cell cycle. Phosphorylation of this protein triggers the release of the transcription factor E2F from the RB/E2F complex, allowing the transcription of the E2F target genes essential for this process [25, 26]. In bone remodeling, *in vitro* investigations on the endogenous role of Cyclin-D1 in osteoblasts have indicated that osteoblast progression can be maintained by promoting the overexpression of PTEN [27, 28].

In this study, we have demonstrated that the miR-16-5p downregulation may be a key regulator in the faster fracture healing process seen in TBI patients, through the promotion of osteoblast proliferation and the inhibition of apoptosis. Moreover, the suppressive effects of miR-16-5p on Bcl-2 and Cyclin-D1 were also confirmed *in vitro* via dual luciferase reporter assays. Through both *in vitro* and *in vivo* experiments, we have demonstrated that the suppression of miR-16-5p by antagomiR-16-5p could be a potential strategy for the treatment of fractures.

Materials and methods

Ethical aspects

All experiments in animals were conducted in compliance with the Guide for the Care and Use of Laboratory Animals by International Committees.

Human serum samples preparation

Serum from 20 male patients were obtained using venous blood draw from the Union Hospital, Tongji Medical College, Huazhong University of Science and Technology. Eighteen serum were obtained from the these 20 patients and divided into three groups: normal group, fracture group and fracture+TBI group. The mean age of these patients was (39.73±5.13) years. The admitted patients underwent conventional X-ray imaging of fractures, along with the Glasgow Coma Scale (GCS) to identify patients with a TBI, which were ultimately diagnosed on the basis of a GCS score of 9-12 together with CT findings. Those in the fracture-only group had GCS scores of 13 or higher. Any patients with previous histories of bone-related or nervous system diseases, malignant disease, open type III fractures, diabetes, autoimmune diseases, other chronic inflammatory diseases, were excluded, as were any patients with a history of a prolonged use of steroids, non-steroidal anti-inflammatory drugs, immunosuppressive agents, or bisphosphonate therapy. The characteristics of including patients could be seen in **Table 1**. The Committees of Clinical Ethics in the Union Hospital, Tongji Medical College, Hua-zhong University of Science and Technology (Wuhan, China) approved this study, and thorough consent was obtained from all the participants.

Femoral fracture models

A total of 20 male C57BL/6J mice between the ages of 6-8 weeks were obtained from the Center of Experimental Animals, Tongji Medical College, Huazhong University of Science and Technology. Anesthesia was induced with 10% chloral hydrate (300 mg/kg body weight). All procedures were approved by the Animal Care and Use Committee of the institution. A longitudinal incision was made, the underlying muscles were bluntly separated without the removal of the periosteum, as described in a previous study [30]. Then, a femoral mid-diaphyseal transverse osteotomy was performed using a low-speed rotary diamond disk. Then, a 0.45-mm diameter stainless steel X was fixed in the bone marrow of the fractured bones for stabilization. At 14 and 21 days post operation, half of the mice were sacrificed respectively, and the callus at the fracture location was harvested for Western blotting and PCR analysis.

Downregulation of miRNA-16-5p accelerates fracture healing following TBI

Table 1. Clinical information of the patients included in the study

Number	Gender (M/F)	Age (year)	Ethnic group	Fracture (Y/N)	Fracture position	TBI (Y/N)	GCS	Time from injury to operation (day)
Non-fracture patients								
1	M	44	Han	N	-	N	15	-
2	M	44	Han	N	-	N	15	-
3	M	30	Han	N	-	N	15	-
4	M	32	Han	N	-	N	15	-
5	M	38	Han	N	-	N	15	-
6	M	45	Han	N	-	N	15	-
Fracture patients								
7	M	45	Han	Y	Tibia	N	15	7
8	M	45	Han	Y	Tibia	N	15	6
9	M	42	Han	Y	Femur	N	14	7
10	M	31	Han	Y	Humerus	N	14	5
11	M	31	Han	Y	Humerus	N	14	6
12	M	42	Han	Y	Radius	N	15	5
Fracture concurrent with TBI patients								
13	M	36	Han	Y	Tibia	Y	8	9
14	M	44	Han	Y	Femur	Y	10	8
15	M	45	Han	Y	Vertebra	Y	9	9
16	M	41	Han	Y	Lumbar	Y	8	9
17	M	30	Han	Y	Patella	Y	10	9
18	M	33	Han	Y	Vertebra	Y	12	10

Abbreviations: M, Male; F, Female; Y, Yes; N, No; TBI, Traumatic brain injury; GCS, Glasgow coma scale.

Fracture concomitant with TBI mouse models

Twenty mice were modeled as fractures with concomitant TBI by using the weight-drop device [31]. After anesthetizing the mice as previously described, they were placed on a platform under a weight drop, and a 1.0-cm longitudinal incision was performed in the midline of the scalp. A micro power drill was used to expose the skull. Once the target impact area was fully exposed (1.5 mm lateral to the midline on the mid-coronal plane), a weight of 20 N was released from a 20-cm height to produce a brain injury. Finally, the mice were returned to their quondam cages after closing their scalp wounds.

micro-CT analysis

Fracture sites were evaluated using a micro-CT system BRUKER SkyScan 1176 scanner to provide images at a configuration of 2400 views, 5 frames per view, 37 kV, and 121 Ma. These images were then analyzed with Bruker micro-CT evaluation software in several aspects, including the segmentation, 3D morphometry, density, and distance parameters (BRUKER,

Germany). Briefly, the bones were thoroughly cleaned off soft tissues before micro-CT. Various 3D structural aspects were analyzed, including Tb.N, BV/TV per tissue volume, Tb.Th, Tb.Sp, average cortical thickness (Ct.Th), cortical area fraction (Ct.Ar/Tt.Ar), cortical bone area (Ct.Ar), total cross-sectional area (Tt.Ar), and BMD. After scanning, the callus' miRNA were extracted for PCR and Western blotting.

Cell culture and transfection

MC3T3-E1 cells-a mouse osteoblast cell line-were contributed by the Huazhong University of Science and Technology, Wuhan, China. The α-MEM (Hyclone) was supplemented with 10% fetal bovine serum (FBS) (Gibco), 1% penicillin and streptomycin (Hyclone) for cell culture at the incubation conditions of 37°C with 5% CO_2 and 95% relative humidity. Cell cultures beyond the sixth passage were not used for further analyses. Lipofectamine TM 3000 (ThermoFisher Scientific, USA) was used for the transfection of agomiR-16-5p, agomiR-NC, antagomiR-16-5p and antagomiR-NC (GenePharma Shanghai) at a concentration of 20 µM according to the manufacturer's instructions. Bcl-2

Table 2. miRNAs and mRNA primer sequence

microRNAs or gene name	Primer sequence (5' to 3')
Mmu-miR-16-5p-Forward	GATCACGATAGCAGCACGTAAA
Mmu-miR-16-5p-Reverse	CTCAACTGGTGTCGTGGAGTC
Mmu-miR-U6-Forward	CTCGCTTCGGCAGCACAT
Mmu-miR-U6-Reverse	AACGCTTCACGAATTTGCGT
Hsa-miR-16-5p-Forward	TGGGGTAGCAGCACGTAAA
Hsa-miR-16-5p-Reverse	CTCAACTGGTGTCGTGGAGTC
Hsa-miR-U6-Forward	CTCGCTTCGGCAGCACAT
Hsa-miR-U6-Reverse	AACGCTTCACGAATTTGCGT
Mmu-BCL2-Forward	GATTGTGGCCTTCTTTGAGTTC
Mmu-BCL2-Reverse	CATATAGTTCCACAAAGGCATCC
Mmu-CyclinD1-Forward	GGATGAGAACAAGCAGACCATC
Mmu-CyclinD1-Reverse	AGAAAGTGCGTTGTGCGGTA
Mmu-GAPDH-Forward	TGAAGGGTGGAGCCAAAAG
Mmu-GAPDH-Reverse	AGTCTTCTGGGTGGCAGTGAT

Abbreviations: miR-16-5p, microRNA-16-5p; RT-qPCR, reverse transcription quantitative polymerase chain reaction.

siRNA and Cyclin-D1 siRNA (RIBOBIO Guangzhou) were transfected at a concentration of 50 nM.

Dual luciferase reporter gene assay

The mouse Bcl-2 and Cyclin-D1 3'UTR containing the miR-16-5p binding sequence for the Bcl-2 and Cyclin-D1 genes were amplified from the mouse genomic DNA using PCR. The product was then subcloned downstream of the stop codon in a pGL3 vector (Promega). A Quik Change Site-Directed Mutagenesis Kit (Stratagene) was used to insert mutations in the binding-region as per the manufacturer's instructions. MC3T3-E1 cells were then transiently transfected (2.5×10^5 cells/well) in 24-well plates with Lipofectamine 3000 (ThermoFisher Scientific, USA) following the manufacturer's instructions. 100 ng of the luciferase constructs and 10 ng of the pRL-TK (Promega) Renilla luciferase plasmid were co-transfected. A dual luciferase reporter assay (Promega) was performed following the manufacturer's instructions. A luminometer (Glomax, Promega) was used to quantify luminescence, normalizing each value from the firefly luciferase construct to the corresponding Renilla signal.

Quantitative real-time polymerase chain reaction

The calluses from mice with fracture alone and mice with fracture and TBI were preserved with RNA Later (QIAGEN) until miRNA extraction. The miRNA extraction was performed utilizing TRIzol reagent (Invitrogen), as per the manufacturer's instructions. cDNA was obtained using a one-step Prime Script miRNA cDNA synthesis kit. Then, equal amounts of cDNA were amplified using SYBR Premix Ex TaqII (TaKaRa, Japan). Parameters for the reaction were set to: 95°C for 5 minutes, followed by 40 10-second cycles at 95°C, and 1 minute at 60°C. After reverse transcription, qPCR analysis was carried out on the Thermal Cycler C-1000 Touch system (Bio-Rad CFX Manager, USA). Relative mRNA and miRNA expression levels were assessed individually by the $2^{-\Delta\Delta CT}$ method, utilizing GADPH and U6 as controls. Data were expressed as fold changes compared to their respective controls. **Table 2** shows the primer sequences.

Western blotting

For each group, the harvested samples were lysed on ice using a lysis buffer (Sigma, Switzerland) with 1% protease inhibitor (Thermo-Fisher Scientific, USA). Protein was quantified using a bicinchoninic acid (BCA) protein assay kit (Yeasen Biotechnology Co, Ltd, Shanghai, China), with correction according to quantitative results. Subsequently, the protein fractions were transferred onto an NC membrane (PALL, USA). Following treatment with 5% skim milk, the membrane was incubated with 15 specific antibodies at 4°C overnight, and followed by the addition of an HRP-labeled secondary antibody (CoWin Bioscience, Beijing, China). Visualization was performed via chemiluminescence (Progma, USA). The primary antibodies used were anti-collagen I (1:500, Abcam, USA), anti-Bcl-2 (1:1,000, Abcam, USA), and anti-Cyclin-D1 (1:500, Abcam, USA). All experiments were performed in triplicates.

3-(4,5-Dimethylthiazol-2-yl)-2, 5-diphenyltetrazolium bromide assay

Cells were plated onto a 96-well plate with culture conditions of 5% CO_2 at 37°C for 24, 48, 72, and 96 hours. Subsequently, the samples were subjected to 2 h of incubation at 37°C. The absorbance was observed for each sample at 450 nm (Nanjing Jiancheng Bioengineering Institute, Nanjing, China). Optical density (OD) values of all the wells were estimated using a microplate reader at a wavelength of 450 nm.
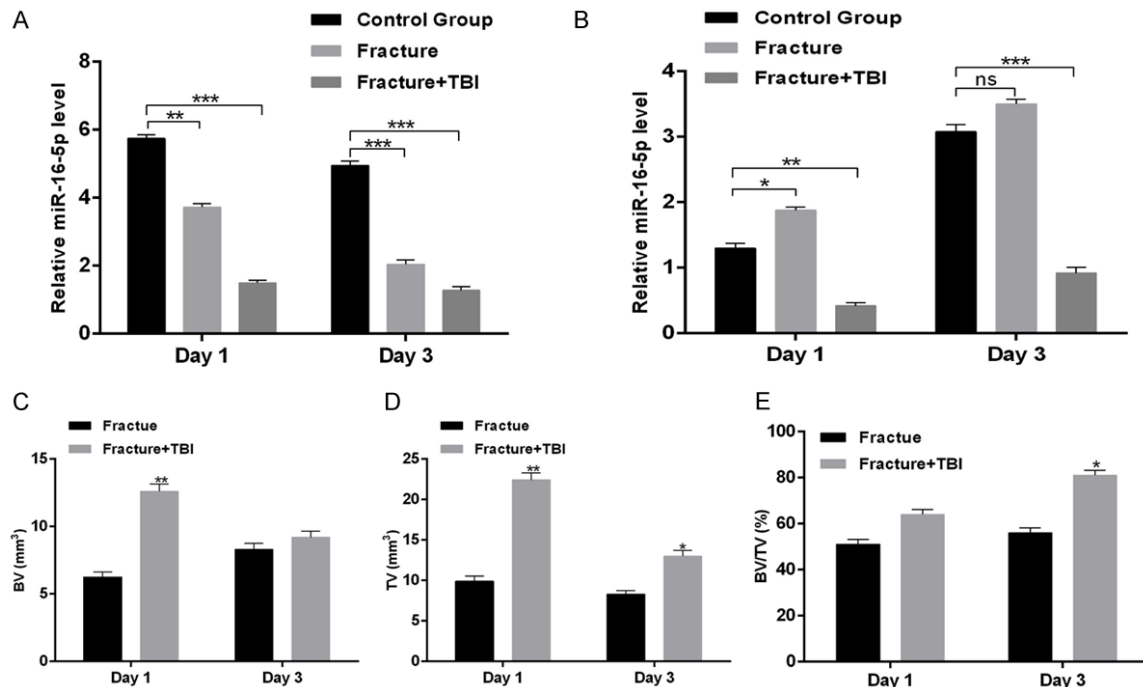
Figure 1. Downregulation of miR-16-5p in TBI patients and animal models. (A) Relative expression level of miR-16-5p of serum sample in each group of patients. (B) Relative expression level of miR-16-5p of serum sample in each group of mice. (C-E) BV (C) and TV (D) of the callus, and BV/TV. All data were expressed as means ± SD. Significance is noted at these thresholds: *P < 0.05, **P < 0.01, ***P < 0.001. One-way ANOVA with a post hoc test was performed. Statistical differences between two groups were determined by Student's t test. n = 10 patients in each group. micro-CT, micro-computed tomography; TV, total volume; BV, bone volume; HE, hematoxylin and eosin.

In the cell growth curve, time was placed in the abscissa and the OD value was placed in the ordinate.

Flow cytometry

Cells treated with ethylene diamine tetra-acetic acid (EDTA)-free trypsin were collected in flow tubes 48 hours following transfection. Supernatant was discarded after centrifugation. Subsequently, PBS was used to wash the cells thrice, while discarding the supernatant after every wash. Cells were then suspended in 0.1 mL RNase A (1 mg/mL) and 0.4 mL propidium iodide (PI) (50 μg/mL) for 10 min. Flow cytometry (FC) was then performed to estimate the proportion of cells in different stages of the cell cycle. Staining was performed for 20 min using calcein-AM and PI solutions for the apoptosis assay, followed by inverted fluorescent microscopy. PI-stained (dead, red) and calcein-AM-stained (live, green) cells were quantified in five randomly-selected fields by three independent observers. Mean values from these observations were used for further analysis.

Statistical analysis

Data are expressed as means ± SD. One-way analysis of variance with Tukey's post-hoc test was applied to compare three or more groups and two-tailed Student's t-test was applied to compare data between two groups. Differences were considered statistically significant when P < 0.05. GraphPad Prism 7.0 (GraphPad Software, Inc, La Jolla, CA) was used for all analyses unless otherwise noted.

Results

The involvement of miR-16-5p in the regulation of cell proliferation and apoptosis has been widely studied [32]. Serum miR-16-5p levels were measured using real-time PCR in thirty patients which were divided into three groups (control, fracture, and fracture+TBI). In order to decrease confounding factors, all serum samples were collected from male patients with ages between 35 and 50 years. Compared to the fracture-only group, the fracture+TBI group had significantly lower serum miR-16-5p levels at 24 h and 72 h post-injury (**Figure 1A**).
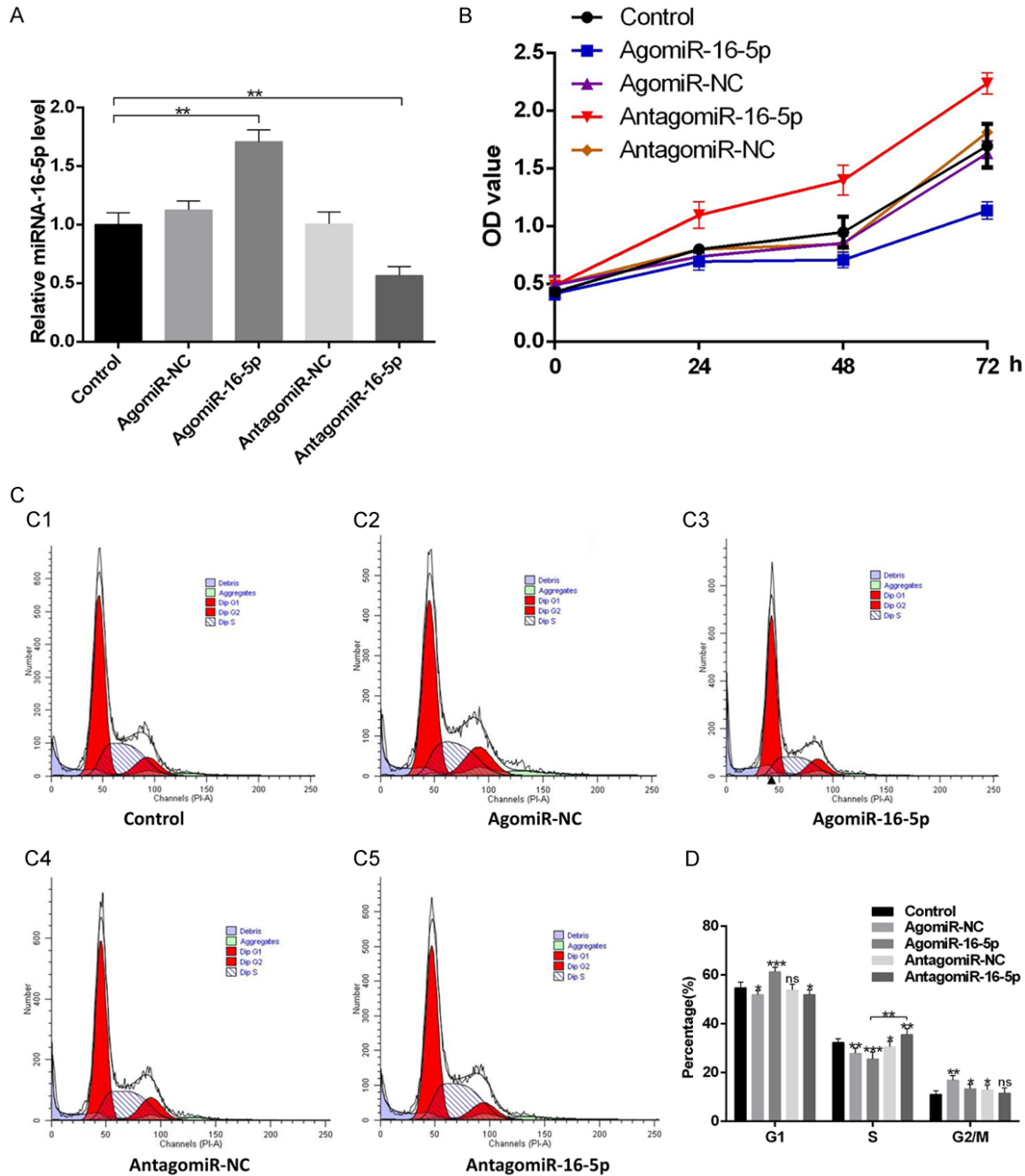
Figure 2. Downregulation of miR-16-5p accelerates osteoblast proliferation in vitro. A. Relative expression of miR-16-5p in MC3T3-E1 cells after transfection with control, agomiR-NC, agomiR-16-5p, antagomiR-NC and antagomiR-16-5p. B. Cytotoxicity of miR-16-5p on MC3T3-E1 cells. C. The distribution of cell cycles after 24 h treatment. D. Downregulation of miR-16-5p induced antagomiR-16-5p-treated cell cycle arrest at the S-G2/M phase. All data were expressed as means ± SD. Significance is noted at these thresholds: *P < 0.05, **P < 0.01, ***P < 0.001. One-way ANOVA with a post hoc test was performed. Statistical differences between two groups were determined by Student's t test.

Also, serum miR-16-5p levels were measured using real-time PCR in mice models of isolated fracture and fracture+TBI. The levels were found to be significantly lower in the fracture+TBI mice model at 24 h and 72 h post-injury (**Figure 1B**). In addition, the trabecular bone microstructure and the femur characteristics from the fracture and fracture+TBI mice models

were evaluated with quantitative micro-computed tomography (micro-CT), including parameters such as trabecular bone volume (BV/TV), trabecular number (Tb.N), trabecular separation (Tb.Sp), and trabecular thickness (Tb.Th). We found that the total volume and bone volume of the callus were significantly higher in the fracture+TBI group at day 14 post-fracture. However, we observed that both the parameters were similar between the groups on day 21 post-fracture; as remodeling had now occurred in the compound group (**Figure 1C-E**).

Downregulation of miR-16-5p promotes osteoblast proliferation in vitro

To explore whether miR-16-5p influences proliferation in osteoblasts, MC3T3-E1 cells were subjected to various treatments in different groups: A control group (Lipofectamine 3000 only), an agomiR-negative control group (agomiR-NC), an agomiR-16-5p group, an antagomiR-negative control group (antagomiR-NC), and an antagomiR-16-5p group. Downregulation of miR-16-5p was observed in the osteoblasts transfected with antagomiR-16-5p (MC3T3-E1+antagomiR-16-5p), in comparison with the other groups (**Figure 2A**). MTT assay was used to characterize the role of miR-16-5p in osteoblast proliferation. We found that the cell growth was faster in the antagomiR-16-5p group but slower in the agomiR-16-5p group as compared to the control, agomiR-NC and antagomiR-NC groups ($P < 0.05$) (**Figure 2B**).

All groups were also examined with FC and PI staining to evaluate the staging and cell division of the cell cycle. We found that the proportion of cells in the S phase were significantly larger in the antagomiR-16-5p group than in the other groups (**Figure 2C**, **2D**). This suggests that antagomiR-16-5p may stimulate cell cycle progression.

Downregulation of miR-16-5p inhibits osteoblast apoptosis in vitro

Flow cytometry was used to assess the role of miR-16-5p in the regulation of osteoblast apoptosis. Staining with annexin V-FITC and PI revealed that the apoptosis rate was higher in the agomiR-16-5p and lower in the antagomiR-16-5p group ($P < 0.05$) as compared to the control, agomiR-NC and antagomiR-NC groups

(**Figure 3A**, **3B**). This suggests that miR-16-5p downregulation potentiated osteoblast resistance to apoptosis.

miR-16-5p directly targets and is negatively associated with Bcl-2 and Cyclin-D1

To investigate whether miR-16-5p directly targets Bcl-2 and Cyclin-D1, luciferase reporters were constructed with either a wild-type (WT) Bcl-2/Cyclin-D1 3'UTR, or a mutant-type (Mut) Bcl-2/Cyclin-D1 3'UTR (**Figure 4A**). Furthermore, MC3T3-E1 cells were also co-transfected with luciferase reporter constructs and antagomiR-16-5p nucleotides. Luciferase activities in both the WT Bcl-2/Cyclin-D1 3'UTR and the mutant Bcl-2/Cyclin-D1 3'UTR reporters were significantly increased after exposure to antagomiR-16-5p, while also affecting the activity of the mutant Bcl-2/Cyclin-D1 3'UTR reporters (**Figure 4A**, **4B**).

In vitro, cells were transfected with agomiR-16-5p, agomiR-NC, antagomiR-16-5p, and antagomiR-NC. After continuous culture for 48 h, higher relative levels of Bcl-2 and Cyclin-D1 mRNA were found in the antagomiR-16-5p group when compared to other groups (**Figure 4C**, **4D**). Our previous results showed that serum miR-16-5p levels were decreased after TBI. To further explore the association between miR-16-5p and Bcl-2/Cyclin-D1, serum samples were obtained from animal models with fracture and TBI to evaluate the corresponding mRNA levels. We found a significant increase in Bcl-2 and Cyclin-D1 mRNA levels in the fracture+TBI mice (**Figure 4E**), suggesting a downregulation of miR-16-5p upregulated Bcl-2 and Cyclin-D1.

Downregulation of Bcl-2 and Cyclin-D1 inhibits osteoblast proliferation

We developed Bcl-2 and Cyclin-D1 siRNAs and assessed their effect on osteoblast proliferation and apoptosis to investigate whether these processes were Bcl-2/Cyclin-D1-dependent. For transfection, cells were divided into control, sham siRNA, Bcl-2 siRNA, and Cyclin-D1 siRNA groups. After continuous culture for 48 h, MC3T3-E1 cells were subjected to Western blotting for Bcl-2 and Cyclin-D1 mRNA (**Figure 5A**). In addition, MTT assay was used to explore the role of Bcl-2/Cyclin-D1 in osteoblast proliferation. Our results suggested that cell growth was inhibited in the Bcl-2 siRNA and Cyclin-D1
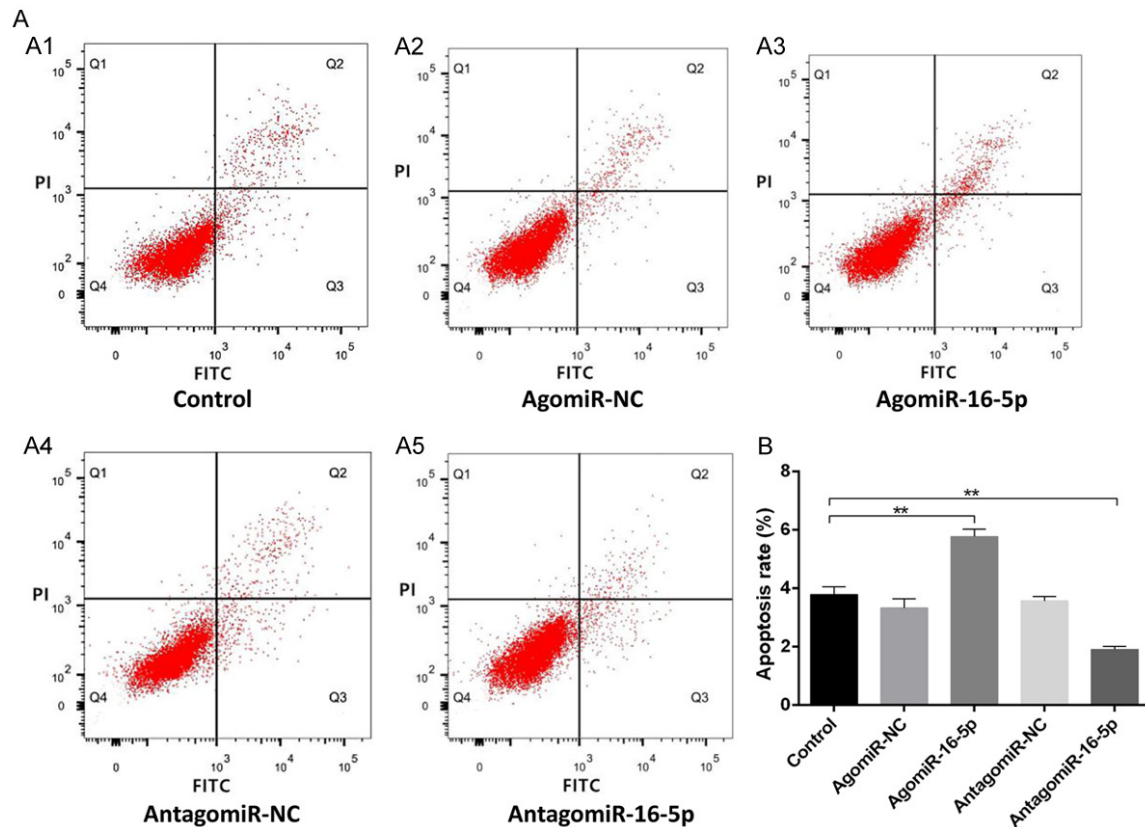
Figure 3. Downregulation of miR-16-5p inhibits osteoblast apoptosis. A. Cell apoptosis of osteoblast in each group. B. Of cell apoptosis rate in each group. All data were expressed as means ± SD. Significance is noted at these thresholds: *P < 0.05, **P < 0.01, ***P < 0.001. One-way ANOVA with a post hoc test was performed. Statistical differences between two groups were determined by Student's t test.

siRNA groups (P < 0.05) (**Figure 5B**). Additionally, FC with PI staining was used to evaluate cell cycle divisions in the control, sham siRNA, Bcl-2 siRNA, and Cyclin-D1 siRNA groups. Results indicated that a significantly smaller proportion of cells were in the S phase of the cell cycle in the Bcl-2 siRNA and Cyclin-D1 siRNA groups than in the other groups (**Figure 5C**, **5D**). Together, these results suggest that osteoblast proliferation may be inhibited by Bcl-2/Cyclin-D1 downregulation.

Downregulation of Bcl-2 and Cyclin-D1 promoted osteoblast apoptosis

The impact of Bcl-2/Cyclin-D1 downregulation in osteoblast apoptosis was assessed with flow cytometry. Staining with Annexin V-FITC and PI revealed a higher apoptosis rate in the siRNA-NC, Bcl-2 siRNA and Cyclin-D1 siRNA groups than in the control and siRNA-NC groups (P < 0.05). This indicates that downregulation of Bcl-2/Cyclin-D1 enhanced the osteoblast apoptosis.

Local administration of antagomiR-16-5p accelerates fracture healing in the femur of mice

Fracture sites were treated with local PBS, agomiR-16-5p and antagomiR-16-5p to assess their impact on fracture healing. Local injection was given on the first day, the third day and the seventh day post-injury. Subsequently, m-CT examination was performed at days 14 and 21 post-injury. Compared to the control and agomiR-16-5p groups, greater callus volumes and smaller fracture gaps were found in the antagomiR-16-5p group (**Figure 7A**). Likewise, the micro-CT showed that the total volume and bone volume of the calluses were greater in the antagomiR-16-5p group than in the control and agomiR-16-5p groups on day 14 post-fracture. Significant differences in these parameters were also found between the agomiR-16-5p and antagomiR-16-5p groups on day 21 post-fracture (**Figure 7B-D**). These findings suggest that miR-16-5p negatively modulates bone remodeling, and its downregulation may accelerate fracture healing.
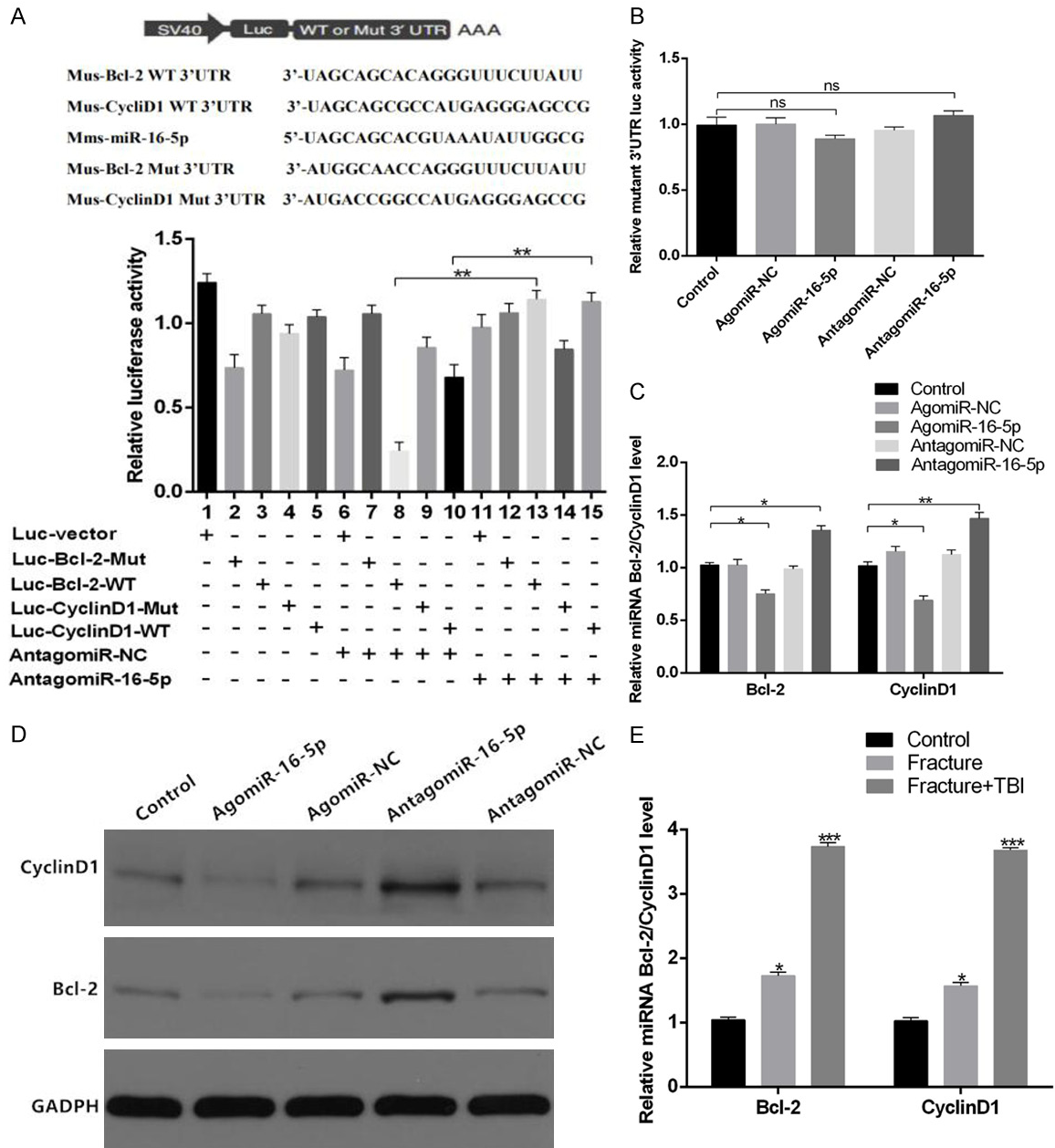
Figure 4. miR-16-5p targets Bcl-2 and Cyclin-D1 to functionally inhibit osteoblast activity in vitro. A. Effect of endogenous miR-16-5p on the luciferase activity of WT Bcl-2/Cyclin-D1 3′UTR (luc-UTR), Bcl-2/Cyclin-D1 3′UTR mutant (luc-UTR-Mut), or the luciferase vector control (luc-vector) after treatment with antagomiR-16-5p in MC3T3-E1 cells. B. Effect of endogenous miR-16-5p on the luciferase activity of WT Bcl-2/Cyclin-D1 3′UTR (luc-UTR), the Bcl-2/Cyclin-D1 3′UTR mutant (luc-UTR-Mut) after treatment with antagomiR-16-5p or its negative control (antagomiR-NC) in MC3T3-E1 cells. C. RT-qPCR analysis of control, agomiR-NC, agomiR-16-5p, antagomiR-NC and antagomiR-16-5p transfection on expression of Bcl-2/Cyclin-D1 protein. D. Western blot analysis of control, agomiR-NC, agomiR-16-5p, antagomiR-NC and antagomiR-16-5p transfection on expression of Bcl-2/Cyclin-D1 protein. E. Bcl-2/Cyclin-D1 expression in serum of mice models. All data were expressed as means ± SD. Significance is noted at these thresholds: *P < 0.05, **P < 0.01, ***P < 0.001. One-way ANOVA with a post hoc test was performed. Statistical differences between two groups were determined by Student's t test. mRNA, messenger RNA; miR-16-5p, microRNA-16-5p; NC, negative control; RT-qPCR, reverse transcription quantitative polymerase chain reaction.

Discussion

Previous research has shown that osteoblast differentiation is regulated by several factors, including miRNAs [33-35]. In particular, miRNA-16-5p has been highlighted as a regulator of cell proliferation and apoptosis [36, 37]. Our results outline the therapeutic potential of miR-
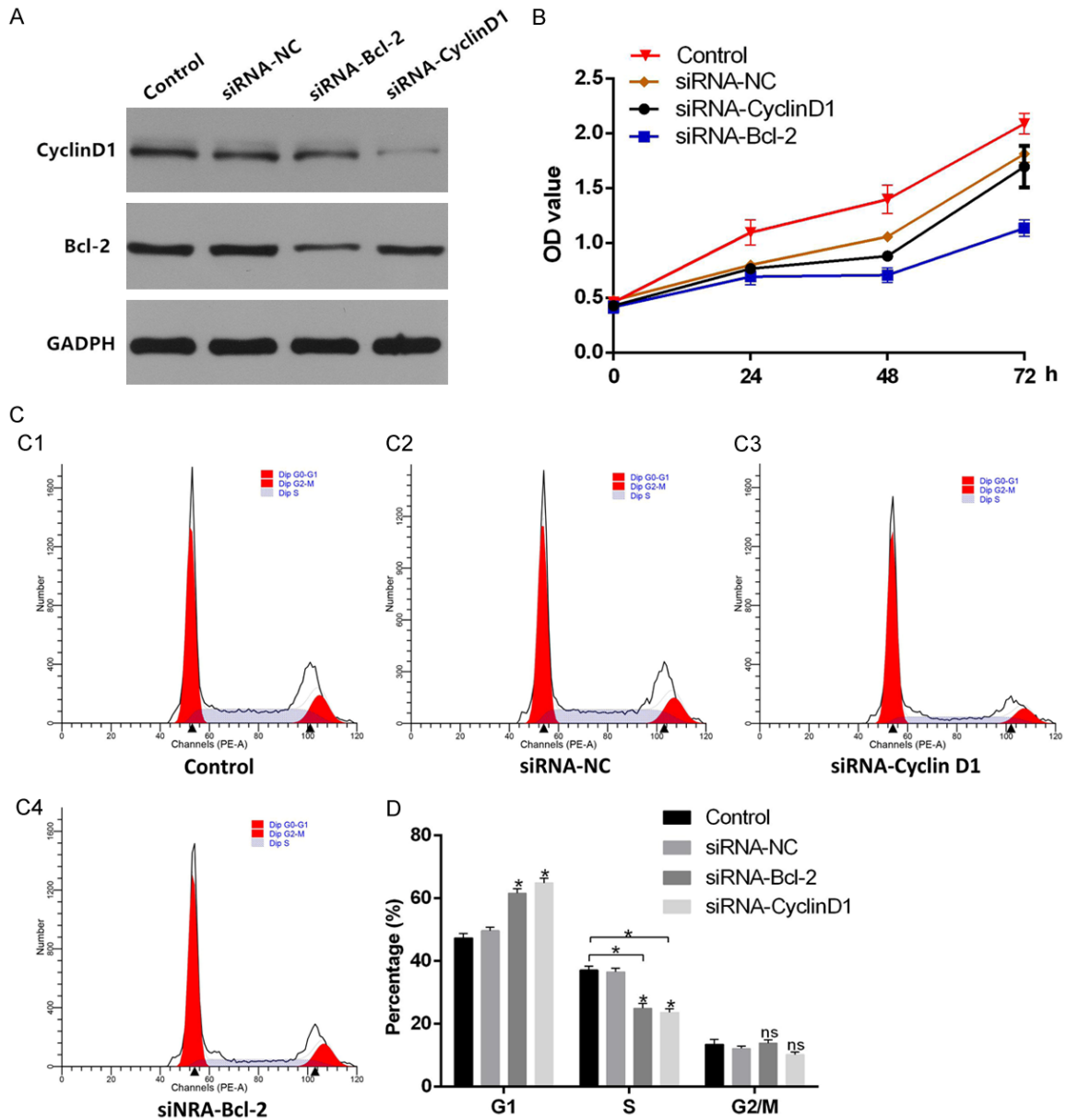
Figure 5. Reduction of Bcl-2/Cyclin-D1 suppressed osteoblast proliferation. A. Western blot analysis of control, siRNA-NC, siRNA-Bcl-2, and siRNA-Cyclin-D1 transfection on expression of Bcl-2 and Cyclin-D1 level. B. Cytotoxicity of Bcl-2/Cyclin-D1 on MC3T3-E1 cells. C. The distribution of cell cycles after 24 h treatment. D. Downregulation of Bcl-2/Cyclin-D1 induced cell cycle arrest at the G1 phase. All data were expressed as means ± SD. Significance is noted at these thresholds: *$P < 0.05$, **$P < 0.01$, ***$P < 0.001$. One-way ANOVA with a post hoc test was performed. Statistical differences between two groups were determined by Student's t test.

NA-16-5p suppression in osteoblasts to accelerate bone remodeling. However, future studies are necessary to investigate the extent to which miRNA-16-5p is activated during bone formation under concurrent TBI.

Several reports in humans, animals, as well as in vitro studies suggest that TBI could accelerate fracture healing [38, 39]. A recent study [40] described upregulation of M2 macropha-

ges following TBI, whose proportions appear to be associated with an accelerated fracture healing in patients with TBI. Furthermore, some researchers [41] have explored the positive effects of TBI on bone healing via histological analyses conducted in mice models, and have also identified the crucial role leptin plays in fracture healing and bone formation, where it was shown that the absence of leptin attenuated the positive effect of TBI on fracture heal-
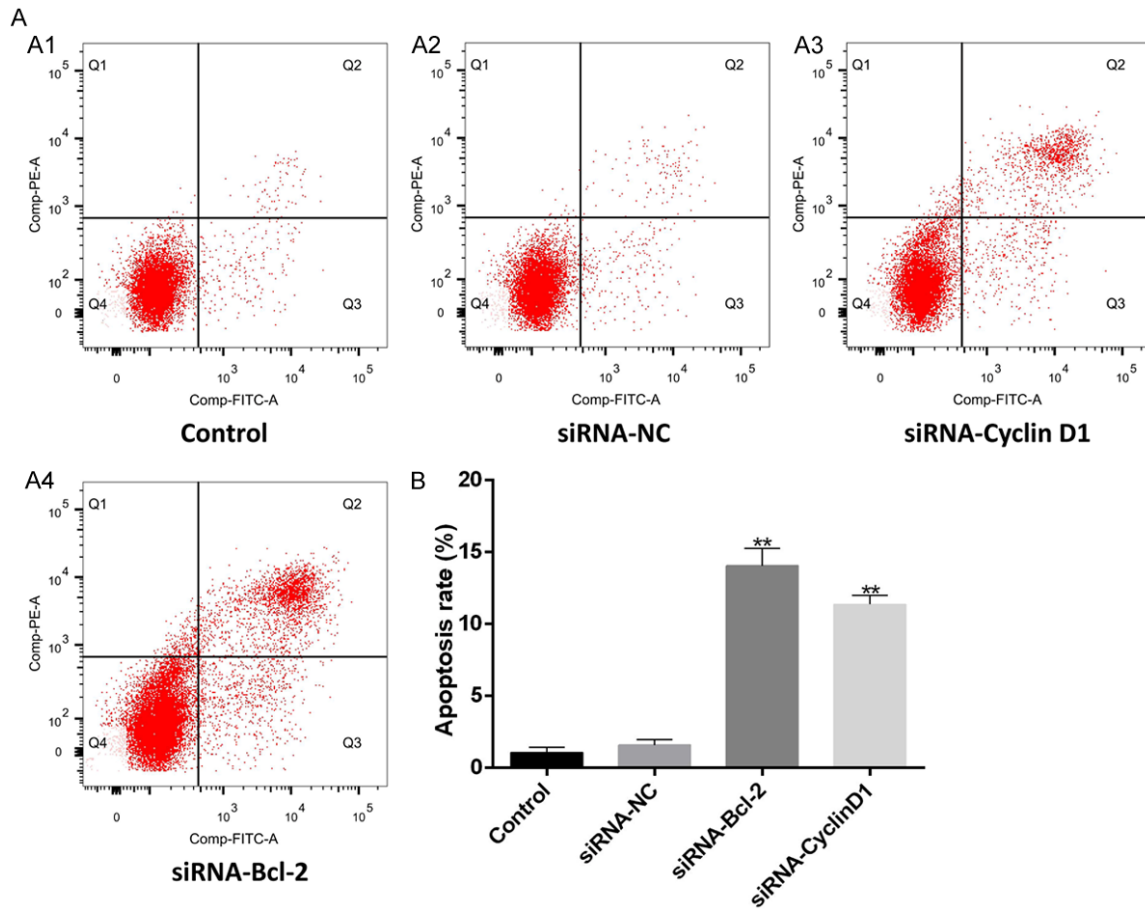
Figure 6. Downregulation of Bcl-2 and Cyclin-D1 enhance apoptosis of osteoblast. A. Cell apoptosis of osteoblast in each group. B. Of cell apoptosis rate in each group. All data were expressed as means ± SD. Significance is noted at these thresholds: *P < 0.05, **P < 0.01, ***P < 0.001. One-way ANOVA with a post hoc test was performed. Statistical differences between two groups were determined by Student's t test.

ing. In addition, many studies have reported that TBI can promote bone healing at the molecular level [42-44]. For example, one study [42] described the SDF-1/CXCR4 axis to be an important accelerator of fracture healing with concomitant TBI, contributing to the endochondral bone repair. In the present study, we have found a significantly improved osteoblast proliferation and bone healing along with the inhibition of osteoblast apoptosis when TBI was present.

Our findings also suggest that with concomitant TBI, Bcl-2 mRNA and Cyclin-D1 mRNA levels increase, with a concurrent downregulation of miRNA-16-5p. In contrast, the overexpression of Bcl-2 mRNA and Cyclin-D1 mRNA levels promoted osteoblast proliferation and inhibited apoptosis. To elucidate the relationship of miR-16-5p with TBI with respect to osteoblast

proliferation and apoptosis, as well as bone formation, potential targets of miR-16-5p were investigated. Our findings showed that 3'UTR of Bcl-2 mRNA Cyclin-D1 mRNA had suitable match sites for the miR-16-5p seed region. Likewise, the decrease in miR-16-5p levels as a consequence of transfection of antagomiR-16-5p led to the upregulation of Bcl-2 and Cyclin-D1. The luciferase reporter experiment showed that miR-16-5p directly targets Bcl-2 and Cyclin-D1 3'UTR. In addition, a negative correlation was found between the Bcl-2 and Cyclin-D1 levels and miR-16-5p. These findings suggest that the latter are physiological targets for miR-16-5p, displaying an inverse association.

Furthermore, we also verified that inhibition of miR-16-5p by antagomiR-16-5p significantly promoted osteoblast proliferation and inhibi-
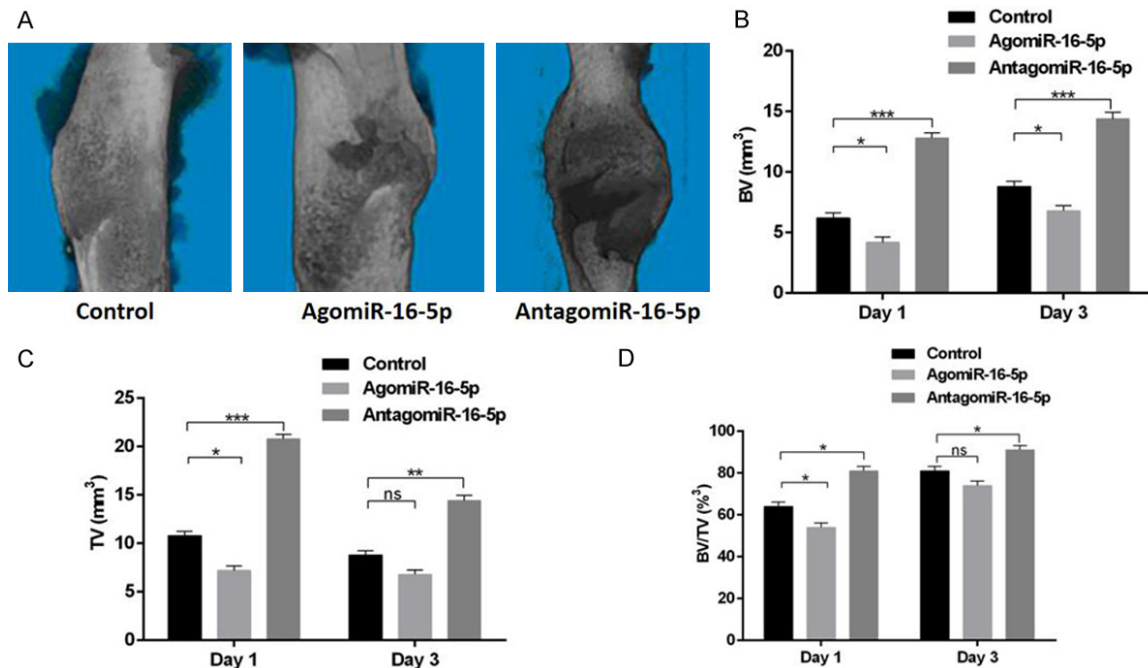
Figure 7. Local administration of antagomiR-16-5p enhanced fracture healing in mice. (A) m-CT image comparison of fracture healing between control, agomiR-16-5p, and antagomiR-16-5p group at day 21 after injury. (B-D) BV (B) and TV (C) of the callus, and BV/TV (D) on postoperative day 14 and 21 was quantified using micro- CT. n = 10 mice per group. All data were expressed as means ± SD. Significance is noted at these thresholds: *P < 0.05, **P < 0.01, ***P < 0.001. One-way ANOVA with a post hoc test was performed. Statistical differences between two groups were determined by Student's t test.

ted apoptosis. Our findings in vitro demonstrated that decreasing miR-16-5p levels in the fracture site could accelerate the precipitation within bone formation and healing. These results suggest that the downregulation of miR-16-5p accelerates bone formation with concurrent TBI through a negative feedback mechanism occurring among miR-16-5p, Bcl-2, and Cyclin-D1. Moreover, we have produced a model for the miR-16-5p-mediated inhibition of osteoblast proliferation and promotion of apoptosis by downregulation of Bcl-2 and Cyclin-D1 (**Figures 4**-**6**). Interestingly, results from the *in vivo* experiment suggested that interruption of Bcl-2 and Cyclin-D1 activity suppressed bone formation by promoting osteoblast apoptosis and inhibiting proliferation.

High expression of miR-16-5p is known to occur in diffuse large B-cell lymphomas, B cell infiltrate tumors, and melanomas, indicating that miR-16-5p participates in immunoreactions as well [45, 46]. However, we could not find studies on the role of miR-16-5p in bone formation. In the present study, we have identified a mechanism for Bcl-2 and Cyclin-D1 regulation by miR-16-5p in osteoblast proliferation and apop-

tosis. In recent years, studies have indicated that miRNAs act as significant regulators of bone remodeling and possibly of human bone disorders [47-49]. These molecules can regulate mRNA at the level of their targets, and the suppression of miRNAs by antagomiRNAs could modulate several mRNAs [50]. However, the function of specific miRNAs on osteoblast proliferation and apoptosis with concomitant TBI condition remains unidentified.

We observed that the downregulation of miR-16-5p in TBI is linked to a concurrent overexpression of Bcl-2 and Cyclin-D1, as observed in MC3T3-E1 cells. Underlying mechanisms were explored by investigating the miR-16-5p target genes. Results showed that a decline in miR-16-5p levels with concurrent TBI resulted in the induction of Bcl-2 and Cyclin-D1. In turn, the overexpression accelerated bone formation by promoting osteoblast proliferation and suppressing apoptosis as the therapeutic inhibition of miR-16-5p *in vivo* in the mice fracture models accelerated fracture healing.

In summary, we found that the suppression of miR-16-5p by antagomiR-16-5p increased os-

teoblast proliferation and decreased apoptosis in MC3T3-E1 cells, pointing towards a potential signaling pathway that may be involved in fracture healing upon concurrent TBI. Thus, the inhibition of miR-16-5p with antagomiR-16-5p and the subsequent increase in Bcl-2 and Cyclin-D1 may be utilized as a potential therapeutic strategy in fracture healing.

Acknowledgements

Disclosure of conflict of interest

None.

Address correspondence to: Bobin Mi and Guohui Liu, Department of Orthopaedics, Union Hospital, Tongji Medical College, Huazhong University of Science and Technology, 1277 Jiefang Avenue, Wuhan 430022, China. E-mail: mi19882@163.com (BBM); liuguohui@hust.edu.cn (GHL)

References

[1] Wildburger R, Zarkovic N, Egger G, Petek W, Zarkovic K, Hofer HP. Basic fibroblast growth factor (BFGF) immunoreactivity as a possible link between head injury and impaired bone fracture healing. Bone Miner 1994; 27: 183-192.

[2] Cai P, Cai T, Li X, Fan L, Chen G, Yu B, Liu T. Herbacetin treatment remitted LPS induced inhibition of osteoblast differentiation through blocking AKT/NF-kappaB signaling pathway. Am J Transl Res 2019; 11: 865-874.

[3] Gu Z, Long J, Li Y, Wang X, Wang H. MiR-125a-3p negatively regulates osteoblastic differentiation of human adipose derived mesenchymal stem cells by targeting Smad4 and Jak1. Am J Transl Res 2019; 11: 2603-2615.

[4] Song D, Xu P, Liu S, Wu S. Dental pulp stem cells expressing SIRT1 improve new bone formation during distraction osteogenesis. Am J Transl Res 2019; 11: 832-843.

[5] Garland DE. Clinical observations on fractures and heterotopic ossification in the spinal cord and traumatic brain injured populations. Clin Orthop Relat Res 1988; 86-101.

[6] Vi L, Baht GS, Soderblom EJ, Whetstone H, Wei Q, Furman B, Puviindran V, Nadesan P, Foster M, Poon R, White JP, Yahara Y, Ng A, Barrientos T, Grynpas M, Mosely MA, Alman BA. Macrophage cells secrete factors including LRP1 that orchestrate the rejuvenation of bone repair in mice. Nat Commun 2018; 9: 5191.

[7] Einhorn TA, Gerstenfeld LC. Fracture healing: mechanisms and interventions. J Nat Rev Rheumatol 2015; 11: 45-54.

[8] Ducy P, Schinke T, Karsenty G. The osteoblast: a sophisticated fibroblast under central surveillance. Science 2000; 289: 1501-1504.

[9] Zhang J, Wan Q, Yu X, Cheng G, Ni Y, Li Z. Low-dose nicotine reduces the homing ability of murine BMSCs during fracture healing. Am J Transl Res 2018; 10: 2796-2809.

[10] Liu H, Su H, Wang X, Hao W. MiR-148a regulates bone marrow mesenchymal stem cells-mediated fracture healing by targeting insulin-like growth factor 1. J Cell Biochem 2018; [Epub ahead of print].

[11] Yao CJ, Lv Y, Zhang CJ, Jin JX, Xu LH, Jiang J, Geng B, Li H, Xia YY, Wu M. MicroRNA-185 inhibits the growth and proliferation of osteoblasts in fracture healing by targeting PTH gene through down-regulating Wnt/beta-catenin axis: in an animal experiment. Biochem Biophys Res Commun 2018; 501: 55-63.

[12] Nugent M. MicroRNAs and fracture healing. Calcif Tissue Int 2017; 101: 355-361.

[13] Strassburg S, Nabar N, Lampert F, Goerke SM, Pfeifer D, Finkenzeller G, Stark GB, Simunovic F. Calmodulin regulated spectrin associated protein 1 mRNA is directly regulated by miR-126 in primary human osteoblasts. J Cell Biochem 2017; 118: 1756-1763.

[14] Li Y, Fan L, Hu J, Zhang L, Liao L, Liu S, Wu D, Yang P, Shen L, Chen J, Jin Y. MiR-26a rescues bone regeneration deficiency of mesenchymal stem cells derived from osteoporotic mice. Mol Ther 2015; 23: 1349-1357.

[15] Hadjiargyrou M, O'Keefe RJ. The convergence of fracture repair and stem cells: interplay of genes, aging, environmental factors and disease. J Bone Miner Res 2014; 29: 2307-2322.

[16] Jia HL, Zhou DS. Downregulation of microRNA-367 promotes osteoblasts growth and proliferation of mice during fracture by activating the PANX3-mediated Wnt/beta-catenin pathway. J Cell Biochem 2018; [Epub ahead of print].

[17] Arfat Y, Basra M, Shahzad M, Majeed K, Mahmood N, Munir H. miR-208a-3p suppresses osteoblast differentiation and inhibits bone formation by targeting ACVR1. Mol Ther Nucleic Acids 2018; 11: 323-336.

[18] Zhang XH, Geng GL, Su B, Liang CP, Wang F, Bao JC. MicroRNA-338-3p inhibits glucocorticoid-induced osteoclast formation through RANKL targeting. Genet Mol Res 2016; 15.

[19] Fushimi S, Nohno T, Nagatsuka H, Katsuyama H. Involvement of miR-140-3p in Wnt3a and TGFbeta3 signaling pathways during osteoblast differentiation in MC3T3-E1 cells. Genes Cells 2018; 23: 517-527.

[20] Zha X, Sun B, Zhang R, Li C, Yan Z, Chen J. Regulatory effect of microRNA-34a on osteogenesis and angiogenesis in glucocorticoid-induced osteonecrosis of the femoral head. J Orthop Res 2018; 36: 417-424.

[21] Seenprachawong K, Tawornsawutruk T, Nantasenamat C, Nuchnoi P, Hongeng S, Supokawej A. miR-130a and miR-27b enhance osteogenesis in human bone marrow mesenchymal stem cells via specific down-regulation of peroxisome proliferator-activated receptor gamma. Front Genet 2018; 9: 543.

[22] Cheng Y, Tang Q, Li Y, Zhang Y, Zhao C, Yan J, You H. Folding/unfolding kinetics of G-quadruplexes upstream of the P1 promoter of the human BCL-2 oncogene. J Biol Chem 2019; 294: 5890-5895.

[23] Greenhough J, Papadakis ES, Cutress RI, Townsend PA, Oreffo R, Tare RS. Regulation of osteoblast development by Bcl-2-associated athanogene-1 (BAG-1). Sci Rep 2016; 6: 33504.

[24] Moriishi T, Fukuyama R, Miyazaki T, Furuichi T, Ito M, Komori T. Overexpression of BCLXL in osteoblasts inhibits osteoblast apoptosis and increases bone volume and strength. J Bone Miner Res 2016; 31: 1366-1380.

[25] Tanaka T, Kubota M, Shinohara K, Yasuda K, Kato JY. In vivo analysis of the cyclin D1 promoter during early embryogenesis in Xenopus. Cell Struct Funct 2003; 28: 165-177.

[26] Ru Y, Chen XJ, Zhao ZW. Cyclin-D1 and p57 (kip2) as biomarkers in differentiation, metastasis and prognosis of gastric cardia adenocarcinoma. Oncotarget 2017; 8: 73860-73870.

[27] Zhu XB, Lin WJ, Lv C, Wang L, Huang ZX, Yang SW, Chen X. MicroRNA-539 promotes osteoblast proliferation and differentiation and osteoclast apoptosis through the AXNA-dependent Wnt signaling pathway in osteoporotic rats. J Cell Biochem 2018; 119: 8346-8358.

[28] Lee E, Decker AM, Cackowski FC, Kana LA, Yumoto K, Jung Y, Wang J, Buttitta L, Morgan TM, Taichman RS. Growth arrest-specific 6 (GAS6) promotes prostate cancer survival by G1 arrest/S phase delay and inhibition of apoptosis during chemotherapy in bone marrow. J Cell Biochem 2016; 117: 2815-2824.

[29] Fernandez AF, Sebti S, Wei Y. Disruption of the beclin 1-Bcl-2 autophagy regulatory complex promotes longevity in mice. Nature 2018; 558: 136-140.

[30] Morgan EF, Hussein AI, Al-Awadhi BA, Hogan DE, Matsubara H, Al-Alq Z, Fitch J, Andre B, Hosur K, Gerstenfeld LC. Vascular development during distraction osteogenesis proceeds by sequential intramuscular arteriogenesis followed by intraosteal angiogenesis. Bone 2012; 51: 535-545.

[31] Flierl MA, Stahel PF, Beauchamp KM, Morgan SJ, Smith WR, Shohami E. Mouse closed head injury model induced by a weight-drop device. Nat Protoc 2009; 4: 1328-1337.

[32] Zhan XH, Xu QY, Tian R. MicroRNA16 regulates glioma cell proliferation, apoptosis and invasion by targeting Wip1-ATM-p53 feedback loop. Oncotarget 2017; 8: 54788-54798.

[33] Wang Y, Wang K, Hu Z, Zhou H, Zhang L, Wang H, Li G, Zhang S, Cao X, Shi F. MicroRNA-139-3p regulates osteoblast differentiation and apoptosis by targeting ELK1 and interacting with long noncoding RNA ODSM. Cell Death Dis 2018; 9: 1107.

[34] Aquino-Martinez R, Farr JN, Weivoda MM, Negley BA, Onken JL, Thicke BS, Fulcer MM, Fraser DG, van Wijnen AJ, Khosla S, Monroe DG. miR-219a-5p regulates rorbeta during osteoblast differentiation and in age-related bone loss. J Bone Miner Res 2019; 34: 135-144.

[35] Iwamoto N, Fukui S, Takatani A, Shimizu T, Umeda M, Nishino A, Igawa T, Koga T, Kawashiri SY, Ichinose K, Tmai M, Nakamura H, Origuchi T, Chiba K, Osaki M, Jungel A, Gay S, Kawakami A. Osteogenic differentiation of fibroblast-like synovial cells in rheumatoid arthritis is induced by microRNA-218 through a ROBO/Slit pathway. Arthritis Res Ther 2018; 20: 189.

[36] Ye J, Cheng XD, Cheng B, Cheng YF, Chen XJ, Lu WG. MiRNA detection in cervical exfoliated cells for missed high-grade lesions in women with LSIL/CIN1 diagnosis after colposcopy-guided biopsy. BMC Cancer 2019; 19: 112.

[37] Fan T, Mao Y, Sun Q, Liu F, Lin JS, Liu Y, Cui J, Jiang Y. Branched rolling circle amplification method for measuring serum circulating microRNA levels for early breast cancer detection. Cancer Sci 2018; 109: 2897-2906.

[38] Zhang R, Liang Y, Wei S. The expressions of NGF and VEGF in the fracture tissues are closely associated with accelerated clavicle fracture healing in patients with traumatic brain injury. Ther Clin Risk Manag 2018; 14: 2315-2322.

[39] Song Y, Han GX, Chen L, Zhai YZ, Dong J, Chen W, Li TS, Zhu HY. The role of the hippocampus and the function of calcitonin gene-related peptide in the mechanism of traumatic brain injury accelerating fracture-healing. Eur Rev Med Pharmacol Sci 2017; 21: 1522-1531.

[40] Zhang R, Liang Y, Wei S. M2 macrophages are closely associated with accelerated clavicle fracture healing in patients with traumatic brain injury: a retrospective cohort study. J Orthop Surg Res 2018; 13: 213.

[41] Seemann R, Graef F, Garbe A. Leptin-deficiency eradicates the positive effect of traumatic brain injury on bone healing: histological analyses in a combined trauma mouse model. J Musculoskelet Neuronal Interact 2018; 18: 32-41.

[42] Liu X, Zhou C, Li Y, Ji Y, Xu G, Wang X and Yan J. SDF-1 promotes endochondral bone repair during fracture healing at the traumatic brain injury condition. PLoS One 2013; 8: e54077.

[43] Yang S, Ma Y, Liu Y, Que H, Zhu C, Liu S. Arachidonic acid: a bridge between traumatic brain injury and fracture healing. J Neurotrauma 2012; 29: 2696-2705.

[44] Andermahr J, Elsner A, Brings AE, Hensler T, Gerbershagen H, Jubel A. Reduced collagen degradation in polytraumas with traumatic brain injury causes enhanced osteogenesis. J Neurotrauma 2006; 23: 708-720.

[45] Tuncer SB, Akdeniz D, Celik B, Kilic S, Sukruoglu O, Avsar M, Ozer L, Ekenel M, Ozel S, Yazici H. The expression levels of miRNA-15a and miRNA-16-1 in circulating tumor cells of patients with diffuse large B-cell lymphoma. Mol Biol Rep 2019; 46: 975-980.

[46] Sabarimurugan S, Madurantakam Royam M, Das A, Das S, K M G, Jayaraj R. Systematic review and meta-analysis of the prognostic significance of miRNAs in melanoma patients. Mol Diagn Ther 2018; 22: 653-669.

[47] Seeliger C, Balmayor ER, van Griensven M. miRNAs related to skeletal diseases. Stem Cells Dev 2016; 25: 1261-1281.

[48] Baek D, Lee KM, Park KW, Suh JW, Choi SM, Park KH, Lee JW, Kim SH. Inhibition of miR-449a promotes cartilage regeneration and prevents progression of osteoarthritis in in vivo rat models. Mol Ther Nucleic Acids 2018; 13: 322-333.

[49] Wang X, Guo B, Li Q, Peng J, Yang Z, Wang A, Li D, Hou Z, Lv K, Kan G, Cao H, Wu H, Song J, Pan X, Sun Q, Ling S, Li Y, Zhu M, Zhang P, Peng S, Xie X, Tang T, Hong A, Bian Z, Bai Y, Lu A, Li Y, He F, Zhang G, Li Y. miR-214 targets ATF4 to inhibit bone formation. Nat Med 2013; 19: 93-100.

[50] Luo F, Xie Y, Wang Z, Huang J, Tan Q, Sun X, Li F, Li C, Liu M, Zhang D, Xu M, Su N, Ni Z, Jiang W, Chang J, Chen H, Chen S, Xu X, Deng C, Wang Z, Du X, Chen L. Adeno-associated virus-mediated RNAi against mutant alleles attenuates abnormal calvarial phenotypes in an apert syndrome mouse model. Mol Ther Nucleic Acids 2018; 13: 291-302.